Title: Normalization characteristics of unsaturated undisturbed Ili loess with high level of soluble salt contents

Lisi Niu[†,1], Wenyuan Ren[†,1,2], Aijun Zhang[1,2,*], Yuguo Wang[1], Jiamin Zhao[1], Qingyu Zhao[1,3]

1 College of Water Resources and Architectural Engineering, Northwest A&F University, Yangling, Shaanxi 712100, China

2 Key Laboratory of Agricultural Soil and Water Engineering in Arid and Semiarid Areas, Ministry of Education, Northwest A&F University, Yangling, Shaanxi 712100, China

3 Central China Real Estate Limited, Zhengzhou 450004, China

† These authors have contributed equally to this paper.

* Corresponding author. College of Water Resources and Architectural Engineering, Northwest A&F University, Yangling, Shaanxi 712100, China.

E-mail address: zaj@nwsuaf.edu.cn (A.J. Zhang).

Abstract

In order to reveal the mechanical characteristics of the unsaturated undisturbed Ili loess in westerly region, the isotropic compression tests controlling suction, the triaxial shrinkage tests controlling net mean stress and consolidation shear tests controlling net confining pressure and suction were carried out under different soluble salt contents. The objective of investigation is to explore the normalized characteristics of compression curve, soil water characteristic curve and critical state line. The results show that the ratio of void ratio to initial void ratio and the ratio of net mean stress to yield net mean stress are suitable to normalize the compression curves under different suctions in the isotropic compression test. The soil water characteristic curves under different net mean stresses in the triaxial shrinkage test can be normalized by the ratio of water

content to saturated water content and the ratio of suction to air entry value. In the consolidation shear test controlling constant suction, the unsaturated critical state lines under different suctions can be normalized by the corresponding saturated critical state line in the plane of effective net mean stress and deviator stress. The unsaturated critical state lines under different suctions in the plane of void ratio and net mean stress can be normalized by means of degree of gas saturation and the ratio of unsaturated void ratio to saturated void ratio under the same effective net mean stress. The results provide potential benefits for the constructions of large-scale water conservancy projects in the special area of Central Asia.

Keywords

Unsaturated Ili loess; Soluble salt content; Normalization; Compression curve; Soil water characteristic curve; Critical state line

1 Introduction

Central Asia is one of the core areas of the Belt and Road, which is located in the transition region with different climate systems, including the Asian monsoon (Cheng et al., 2012; Dettman et al., 2001), the mid latitude westerly wind (Vandenberghe et al., 2006) and the Arctic polar front (Machalett et al., 2008). Central Asia is also a sensitive area of global climate change. The Ili Basin in China is located in a meso cenozoic fault basin sandwiched by the Tianshan orogenic belt, which belongs to this sensitive area. Ili Basin is bounded by the north and south Tianshan mountains and presents a trumpet shape opening to the west, which is subjected to westerly winds all year round, and its annual average temperature is 2.6~10.4 °C. The precipitation distribution is uneven due to the influence of local topography, which concentrated in the eastern of this area. The research results show that loess is mainly distributed in temperate semi-arid grassland, this is

because the vegetation can intercept the dust in the deposition process and moderate precipitation promotes silty sand deposition. (Tsoar, & Pye, 1987; Dodonov, & Baiguzina, 1995). Therefore, extensive loess deposits exist in the Ili Basin (Song et al., 2014), which is mainly distributed on the windward slopes of mountains on both sides of the valley in terms of distribution characteristics (Li et al., 2012). According to the analysis of material composition, grain size composition (Song et al., 2018), quartz surface morphology (Ye, 2000), and geochemistry (Ye et al., 2005), it has been shown that Ili loess has typical aeolian sedimentary characteristics, which belongs to the typical loess in the westerly region.

In addition, Ili loess with high soluble salt is obviously different from the loess in the loess plateau in the monsoon region. The maximum soluble salt content is 1.92 %, and the maximum self-weight collapsible capacity is 3.52 m by field immersion tests (Zhang et al., 2016). The results show that the global saline alkali land area has reached 9.5×108 hm^2, and the annual growth rate is 1-1.5 million hm^2 (Sumner, & Ravendra, 1998). It is estimated that more than 50 % of cultivated land will be salinized by 2050 (Vinocur, & Altman, 2005). Saline alkali land accounts for 8.16 % of cultivated land in Ili prefecture of China (Wang et al., 2020). The special Ili loess with characteristics of saline soil needs to be studied in a special and systematic way.

In recent years, the research on Ili loess is mainly focused on the aspects of distribution characteristics, ages, dust sources, chemical weathering, particle size, magnetism and mineralogy (Zhang et al., 2013; Song et al., 2014; Yang et al., 2014). Viles, & Goudie (2007) show that the groundwater composition of the site has a great influence on the physical and mechanical characteristics of saline soil. Some scholar explained that the influence mechanism of salt on the soil is more complex from the perspective of comparing the time variation coefficient of salt and

69 water. Yang (2006) pointed out that the unreasonable use of soil resources in arid and semi-arid
70 areas is one of the reasons for accelerating salinization. Due to the migration of water and salt, the
71 salinity distribution in practical engineering is quite different, which causes enormous harm to
72 large-scale water diversion projects, such as canals, slope etc. (Tian et al., 2018; Liu et al., 2019;
73 Turner, & Swenson, 2020; Welegedara et al., 2020). At present, many studies on the loess in
74 monsoon area can be found in literature, but few on the mechanical characteristics of loess in the
75 westerly area, and the Ili loess with the high level of soluble salt content in particular. Therefore,
76 to study the influence of soluble salt on engineering properties of Ili loess will provide insights for
77 the regulation and utilization of water and salt and show benefits for the engineering constructions
78 in saline areas.

79 This paper targets on the Ili loess in China to explore the influence of soluble salt content on
80 the compression, soil water and critical state characteristics. Moreover, the normalization analysis
81 is carried out to obtain the hydraulic and mechanical characteristics of Ili loess considering the
82 influence of soluble salt content. This has important theoretical and application significances in
83 the field of unsaturated loess and special soil, and also can promote the sustainable development
84 of Central Asia and the construction of Belt and Road.

85 **2 Material and test method**

86 2.1 Physical properties and sample preparation

87 The undisturbed loess taken from the Tekes River in Zhaosu, Ili, Xinjiang, China, with depth
88 of 18.5-22 m was used, which is classified as the Late Pleistocene (Q_3) loess. According to the
89 Standard for Soil Test Method of China (GB/T50123-1999), the basic physical properties and
90 initial ion contents of Ili loess were determined, as listed in Table 1.

91 **Table 1** Basic physical properties and initial ion contents of Ili loess

Dry density ρ_d (g·cm^{-3})	Initial water content w_0 (%)	Liquid limit w_l (%)	Plastic limit w_p (%)	Plasticity index I_p (%)	specific gravity Gs	Particle content (%)			Soil classification
						Sand 2-0.075	Silt 0.075-0.005	Clay < 0.005	
1.32-1.41	6.18-6.73	29.2	19.0	10.2	2.72	0.6	76.4	23.0	CL

Depth of soil layer (m)	Ion content (%)								Soluble salt content θ (%)
	HCO_3^-	Cl^-	SO_4^{2-}	Ca^{2+}	Na^+	Mg^{2+}	K^+	CO_3^{2-}	
18.5-19	0.0287	0.0206	0.1228	0.0098	0.1645	0.0073	0	0	0.354
21.5-22	0.0186	0.0354	0.1616	0.0725	0.2338	0.0529	0	0	0.575

According to Table 1, Ili loess is classified as low liquid limit clay (CL). For the soil samples with depths of 18.5-19 m and 21.5-22 m, the initial total soluble salt content is 0.354 % and 0.575 % and the ion content ratio of HCO_3^-:Cl^-:SO_4^{2-}:Ca^{2+}:Na^+:Mg^{2+} is 1:0.7:4.3:0.3:5.7:0.3 and 1:1.9:8.7:3.9:12.6:2.8, respectively. The standard cylindrical samples with diameter of 3.91 cm and height of 8 cm were extracted from the undisturbed soil blocks. Then, the water film transfer method was used to prepare the undisturbed soil samples with different soluble salt contents and water contents, the details of which can be found elsewhere (Wang, Y. G. et al., 2019; Niu et al., 2020).

2.2 Test method

The test equipment is FSY30 stress-strain controlled unsaturated soil triaxial apparatus (Chen et al., 2007). In this paper, three stress path tests were carried out, including the isotropic compression test controlling suction, the triaxial shrinkage test controlling net mean stress and consolidation shear test controlling net confining pressure and suction. Taking one soluble salt content as an example, the test scheme and loading sequence are shown in Table 2.

Table 2 Test scheme and loading sequence (taking one soluble salt content as an example)

Test type	Stress state	Loading process (kPa)
Isotropic compression test	Initial suction	5/ 50/ 100/ 150
	Net mean stress	5→400 (graded loading: ①p < 100 kPa, 20 kPa/ level; ②p≥100 kPa, 50 kPa/ level)
Triaxial shrinkage test	Initial suction	5
	Net mean stress	100
	Suction	5→150 (graded loading: 25 kPa/ level)

Consolidation shear test	Suction	5/ 50/ 100/ 150
	Net confining pressure	100/ 200/ 300

In order to ensure the completion of the tests and the accuracy of the results, the clay plate was saturated before the test and the suction was balanced after the loading of the sample. Five groups of the tests with soluble salt contents of 0.5 %, 0.8 %, 1.4 %, 2 % and 2.6 % were conducted for each stress path test. During each test, the drain valve was opened, and the suction was controlled by applying the pore air pressure. The stability criterion under each load is that the volume change and water discharge are less than 0.006 cm^3 and 0.012 cm^3 within two consecutive hours, respectively. The tests are as follows:

In the isotropic compression test controlling suction, for a certain soluble salt content, 4 tests were carried out under the suction of 5 kPa (saturated sample), 50 kPa, 100 kPa and 150 kPa. In Table 2, the saturated sample is taken as an example. The suction was increased to 5 kPa under the controlled net mean stress of 5 kPa. After the stabilization of load, the suction was controlled as constant, and the net mean stress was gradually loaded to 400 kPa.

In the triaxial shrinkage test controlling net mean stress, for each soluble salt content, the test was completed under the controlled net mean stress of 100 kPa. In Table 2, one salt sample is taken as an example. The net mean stress was increased to 100 kPa under the controlled suction of 5 kPa. After stabilization of the load, the net mean stress was constant, and the suction was gradually loaded to 150 kPa.

In the consolidation shear test controlling net confining pressure and suction, for a certain soluble salt content, a total of 12 tests were conducted with the suction of 5 kPa, 50 kPa, 100 kPa and 150 kPa, and the net confining pressure of 100 kPa, 200 kPa and 300 kPa, respectively. In Table 2, one salt sample is taken as an example. For a single loading stage, the consolidation stage

of the sample was carried out after applying suction and net confining pressure to the target value. When the consolidation was finished, the drainage shear test was then carried out until the axial strain reaching 15 %.

After each test, the drying method was used to measure the final water content of the sample, and the actual water discharge was corrected according to the difference between the initial and the final water content. Although little difference was found, the water discharge in this paper uses the corrected values.

3 Test results and normalized analysis

3.1 Normal compression curve

In the isotropic compression test controlling suction, the curves of void ratio (e) and net mean stress (p) under different suctions are shown in Fig. 1, the soluble salt content of 1.4 % and 2 % are taken as an example. As can be seen from Fig. 1, two straight lines were drawn according to the test points of the same sample. The intersection represents the yield stress point, and the corresponding net mean stress is the structural yield net mean stress (p_c). For a certain soluble salt content, the e-$lg(p)$ curves are different for different suctions, the structural yield net mean stress (p_c) is larger due to the stronger structure under the larger suction. When the stress is larger than p_c, the slope of the e-$lg(p)$ curve is greater, due to the damaged soil structure and reorganized skeleton particles.. The reduction rate of void ratio are then increasing on account of a faster reorganization under a larger suction.

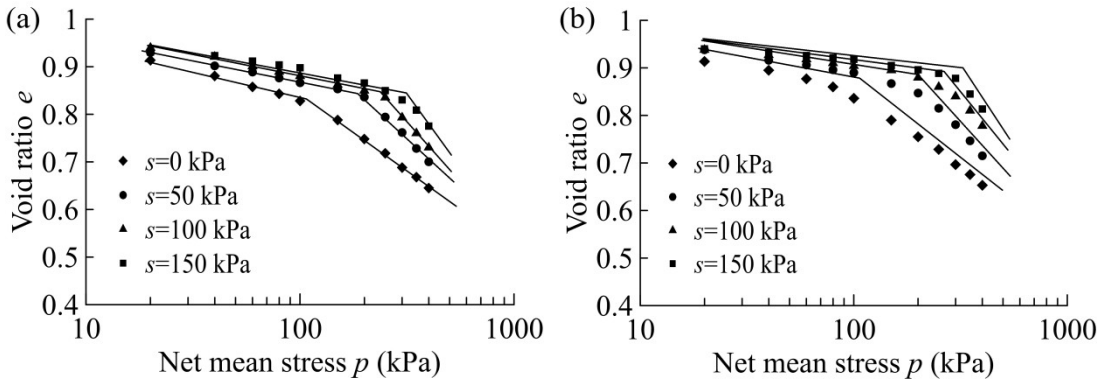

Fig. 1 Curves of void ratio (e) and net mean stress (p) under different suctions: (a) θ=1.4 %; (b) θ=2 %

In this research, the influence of suction on the e-$lg(p)$ relationship was normalized by using parameters reflecting the basic physical and structural properties, such as initial void ratio (e_0) and structural yield net mean stress (p_c). Shao et al. (2017) used the ratio of void ratio to initial void ratio (e/e_0) and the logarithm of the ratio of vertical loading to structural yield net mean stress (p_h/p_c) to normalize the e-p_h curves with different water contents under confined compression condition. The mathematical equations for compression deformation before and after yielding were then established. But it is complicated to express the compression characteristic by polynomial form before yielding. Subsequently, Wang, L. Q. et al. (2019) unified the compression curves before and after yielding as follows:

$$\frac{e}{e_0}=A\exp\left(-\alpha\left(\frac{p_h}{p_c}\right)^{\beta}\right) \tag{1}$$

Where: e_0 and e are the initial void ratio and the void ratio for stabilization under the loading; p_h and p_c are the vertical load and the structural yield net mean stress, respectively; A is the coefficient related to the compression stage, α and β are the soil parameters greater than 0. Eq. (1) effectively simplifies the normalized compression equation, but the different parameters bounded by the value of (p_h/p_c) are required to describe the compression curves before and after yielding. Another scholar (Chen et al., 2017) adopted one curve in the e/e_0-$lg(p_h/p_c)$ plane to normalize the

compacted loess, and the corresponding equation is as follows:

$$\frac{e}{e_0}=\frac{1}{1+a\left(\frac{p_h}{p_c}\right)^b} \tag{2}$$

Where: a and b are soil parameters.

The above Eq. (1) and (2) are established on the basis of the confined compression condition. Whether it is applicable to the results of isotropic compression test needs further verification. Thus the relationship of e/e_0 and p/p_c is proposed in this paper:

$$\frac{e}{e_0}=m\exp\left(-n\left(\frac{p}{p_c}\right)\right) \tag{3}$$

Where: m and n are soil parameters.

Fig. 2 shows the fitting curves of e/e_0 and $lg(p/p_c)$ under different suctions. For a specific soluble salt content, the samples under different suctions show a consistent relationship, indicating that a better normalization by e/e_0-$lg(p/p_c)$ was obtained. Eq. (1)~(3) were then used to fit the results of isotropic compression test under different conditions (see Fig. 2). Here the vertical load (p_h) is replaced by the net mean stress (p), and the fitting parameters of normalization equation of normal compression lines (NCLs) are shown in Table 3.

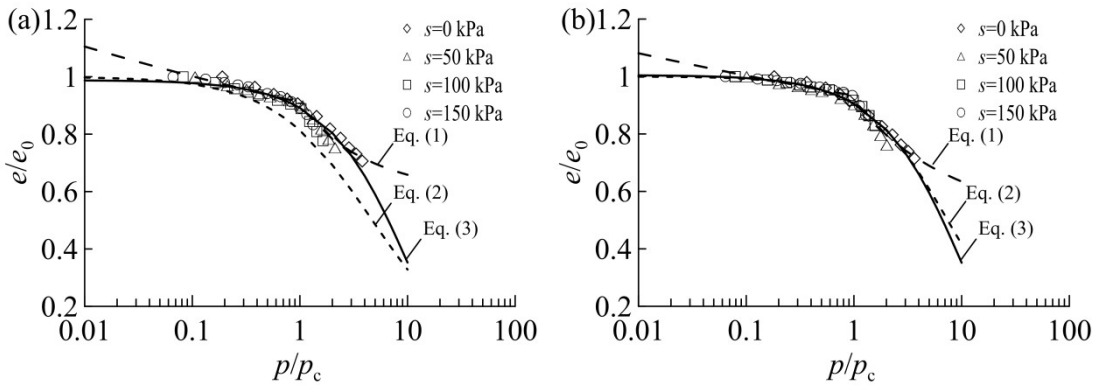

Fig. 2 Fitting curves of e/e_0 and $lg(p/p_c)$ using Eq. (1) ~ (3): (a) θ=1.4 %; (b) θ=2 %

Table 3 Fitting parameters of normalization equation of normal compression lines

Fitting equation	Eq. (1) (Wang, L. Q. et al., 2019)	Eq. (2) (Chen et al.,	Eq. (3)

											2017)
	Parameters	$p/p_c \leq 1$			$p/p_c > 1$						
		A	α	β	A	α	β	a	b	m	n
Soluble salt content θ (%)	0.5	0.29	-1.22	-0.01	0.16	-1.80	-0.11	0.08	0.88	0.97	0.05
	0.8	0.17	-1.72	-0.01	0.29	-1.18	-0.17	0.09	0.91	0.98	0.06
	1.4	0.10	-2.23	-0.02	0.58	-0.44	-0.53	0.23	0.95	0.99	0.10
	2	0.10	-2.20	-0.01	0.46	-0.69	-0.33	0.11	1.12	1.01	0.11
	2.6	0.10	-2.21	-0.01	0.64	-0.35	-0.56	0.10	0.92	0.99	0.08
	R^2	0.69-0.90			0.78-0.94			0.90-0.96		0.85-0.96	

It can be seen from Fig. 2 and Table 3: the values of α and β are less than 0 by using the Eq. (1), which does not meet the aforementioned definition. Both a and b have higher discreteness when the soluble salt content is 1.4 % by using the Eq. (2). The correlation coefficient (R^2) of fitting by Eq. (3) are all above 0.85, and the parameter m with different soluble salt contents varies slightly, so the mean value (m=1) is desirable. That is, Eq. (3) can be simplified to a single-parameter equation including only the parameter n. Fig. 3 shows the relationship between n and soluble salt content. It can be seen that n first increases and then decreases with the increase of soluble salt content. By substituting its equation into Eq. (3), the equation of the normalized compression curve considering soluble salt content can be obtained as follows:

$$\frac{e}{e_0}=\exp\left\{\left(0.04\theta^2-0.13\theta+0.01\right)\left(\frac{p}{p_c}\right)\right\} \quad (4)$$

Where, θ is the soluble salt content (%).

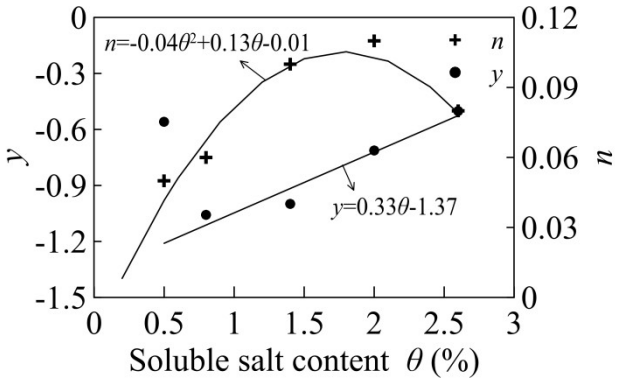

Fig. 3 Curves of parameters n、y and soluble salt content θ

3.2 Soil water characteristic curve (SWCC)

The relationship between suction and degree of saturation or volume water content is used to describe the soil water characteristic. When the volume of the sample is not convenient to be measured, it is more simple to directly use the water content. However, the soil water characteristics of samples under different stress conditions are different. The SWCCs under the same net confining pressure and different levels of shear stress are well normalized, which can be expressed as follows:

$$w/w_s=\left[1+\left(js/s_c\right)^k\right]^{-(1-1/k)} \tag{5}$$

Where: w and w_s are the water content and saturated water content; s and s_c are the suction and air entry value; j and k are the soil parameters.

The above method is utilized to normalize the w-s curves under different net mean stresses. Fig. 4 shows the curves of w/w_s-$lg(s/s_c)$ under different net mean stresses (Gao et al., 2018). It can be seen that the stress points under different net mean stresses are all distributed a narrow range in the plane of w/w_s-$lg(s/s_c)$. The fitting result with high suction using Eq. (5) (the dotted curve in Fig. 4) is not appropriate. Therefore, a better exponential equation is proposed to directly describe the relationship of w/w_s-$lg(s/s_c)$ under different net mean stresses, which can be expressed as:

$$w/w_s=x\exp\left(-ys/s_c\right) \tag{6}$$

Where: x and y are soil parameters.

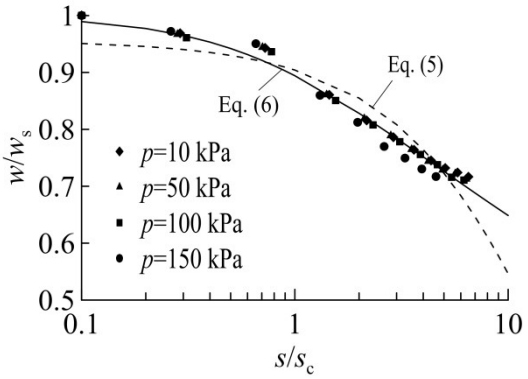

Fig. 4 Curves of w/w_s-$lg(s/s_c)$ under different net mean stresses

It is proofed that the fitting of Eq. (6) is reasonably better (the solid curve in Fig. 4), which is able to normalize the SWCCs under different net mean stresses in the whole suction range. It is worthy to note that the parameters x and y obtained by Eq. (6) are independent of the net mean stress. Thus, the Eq. (6) is used in this paper to fit the SWCCs of different soluble salt contents under three kinds of test methods, and the corresponding parameters obtained are shown in Table 4.

Table 4 Fitting parameters of normalization equation of SWCCs under three kinds of test methods

Test method	Triaxial apparatus method		Centrifuge method (Wang, Y. G. et al., 2019)		Filter paper method (Wang, Y. G. et al., 2019)	
Soluble salt content θ (%)	x	y	x	y	x	y
0.5	1.083	-0.559	0.662	-0.042	2.088	-0.025
0.8	1.148	-1.058	0.685	-0.042	1.988	-0.012
1.4	1.241	-0.999	0.707	-0.058	2.02	-0.013
2	1.144	-0.713	0.705	-0.065	2.038	-0.009
2.6	1.065	-0.502	0.717	-0.046	1.996	-0.005
R^2	0.79-0.97		0.66-0.73		0.74-0.84	

It can be seen that the correlation coefficient (R^2) for the test results of the triaxial apparatus method is larger in comparison with the other two methods, which indicates a better applicability. The parameter x is slightly affected by the soluble salt content, and thus its mean value of 1.14 was taken. The parameter y is approximately linearly correlated with the soluble salt content (see Fig. 3), and the normalized soil water characteristic equation considering soluble salt content can

be obtained by substituting its expression into Eq. (6) as follows:

$$w/w_s = 1.14\exp\left[-(0.33\theta - 1.37)s/s_c\right] \tag{7}$$

Where, θ is the soluble salt content (%).

3.3 Critical state line in *p*-*q* plane

The experimental results show the stress-strain relationship of the samples under different conditions are all hardening type. The stress corresponding to the axial strain of 15 % is taken as the shear failure stresses (q_f and p_f). Fig. 5 shows the shear failure stresses (p_f, q_f) under different suctions in the plane of net mean stress (p) and deviator stress (q). It can be seen from Fig. 5, for a specific suction, the points of shear failure stresses fall on a straight line, which is defined as the critical state line (CSL) in the *p*-*q* plane. The deviator stress (q) increases linearly with the increase of the net mean stress (p) for different suctions, and the CSL is approximately parallel for different suctions and gradually shifts to the upper right with the increase of suction, indicating that the shear failure stresses (both q_f and p_f) are larger under larger suctions.

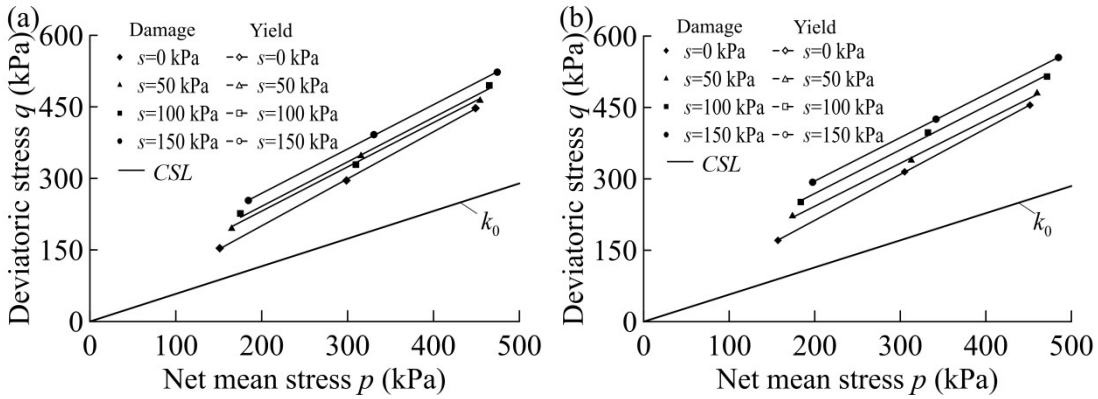

Fig. 5 The shear failure stresses and CSLs under different suctions in the plane of net mean stress and deviator stress: (a) θ=0.8 %; (b) θ=1.4 %

Under the condition of triaxial shear, the equation of the effective net mean stress p' is determined as follows:

$$p' = p + S_r s \tag{8}$$

Where: S_r and s are the degree of saturation and suction of shear failure, respectively. In the plane of effective net mean stress (p') and deviator stress (q), the CSLs with the same soluble salt content under different suctions were normalized, as shown in Fig. 6. For a specific soluble salt content, the stress points of unsaturated undisturbed Ili loess under different suctions are distributed in a narrow area in the p-q' plane, which can approximately be represented by the saturated CSL in the p-q' plane:

$$q = Mp' + c' \tag{9}$$

Where: M and c' are the slope of the saturated CSL and effective cohesion in the p-q plane. This indicates that the strength characteristics of saturated and unsaturated soils follow a consistent rule, which is in line with the references (Nuth, & Laloui, 2008; Chen et al., 2017; Fang, & Feng, 2020). Thus, the Eq. (9) is able to characterize the shear strength characteristics of unsaturated soil only by determining the parameters M and c' of saturated soil, which solves the complex problems of determination for the shear strength of unsaturated soil and adsorption cohesion in the p-q plane, and effectively simplifies the shear strength theory of unsaturated soil.

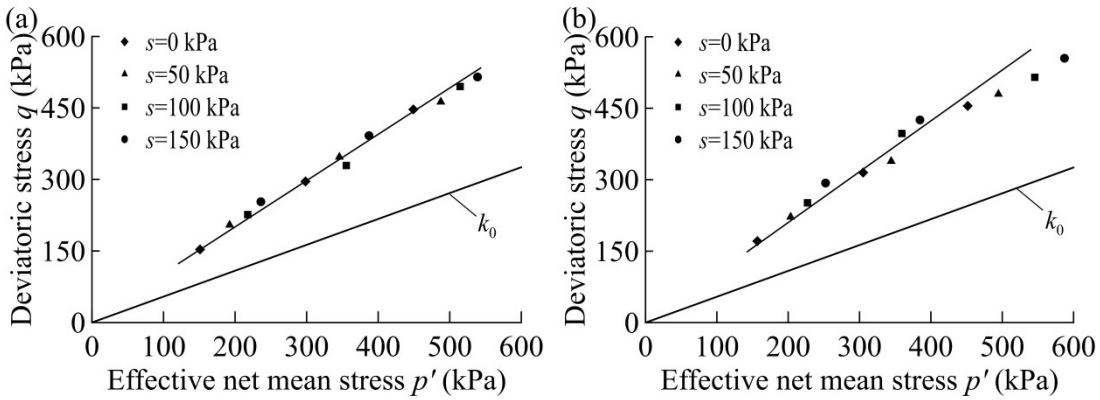

Fig. 6 Normalized CSL in the plane of effective net mean stress and deviator stress: (a) θ=0.8 %; (b) θ=1.4 %

Fig. 7 shows the relationships between slope (M), intercept (c') of the saturated CSL with the soluble salt content. It can be seen that with the increase of soluble salt content, the slope (M) decreases linearly and the effective cohesion (c') first increases and then decreases. Substituting

252 the equations of M and c' into Eq. (9), the normalized CSL considering the influence of soluble
253 salt content is as follows:

254 $$q=(1-0.02\theta)p'+(-9.97\theta^2+32.77\theta-10.72) \quad (10)$$

255 Where, θ is the soluble salt content (%).

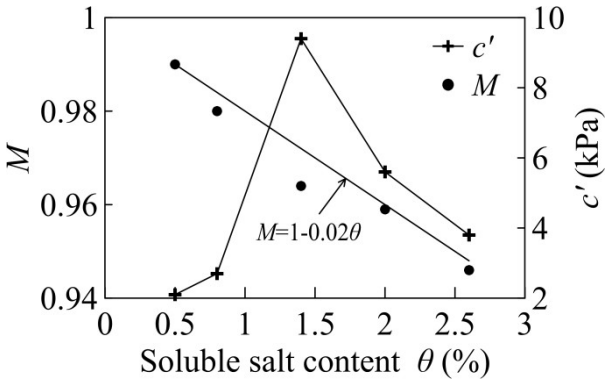

Fig. 7 Relationships between slope (M), intercept (c') of saturated CSL with the soluble salt content (θ)

256 3.4 Critical state line in *e-p* plane

257 Fig. 8 shows the CSLs in the plane of void ratio (e) and net mean stress (p) plane under
258 different conditions. Fig. 8(a) and 8(b) show the CSLs under different suctions, and the
259 corresponding soluble salt content is 0.5 % and 0.8 %. For a specific soluble salt content and
260 suction, the void ratio (e) decreases approximately linearly with the increase of the net mean stress
261 (p). The unsaturated CSL shifts upward as the increase of suction, and its slope is larger than that
262 of the saturated samples, which is consistent with the undisturbed loess under constant water
263 content test condition (Chen et al., 2017).

264 For the samples under the suction of 50 kPa in Fig. 8(c), with the increase of soluble salt
265 content, the void ratio first increases until reaching the maximum under the soluble salt content of
266 1.4 % and then decreases. That is, the CSL first moves up and then down and its slope first
267 decreases and then increases. This is because the higher soluble salt content causes the smaller
268 compressible deformation due to the higher concentration of unsaturated sample. Thus, under the

same net mean stress, the higher soluble salt content results in the larger void ratio and the smaller reduction of void ratio. However, when the soluble salt content is larger than 1.4 %, the crystalized salt particles are becoming the dominant factor rather than the concentration of dissolved salts. The occupation of excess salt particles reduces the void ratio of the sample.

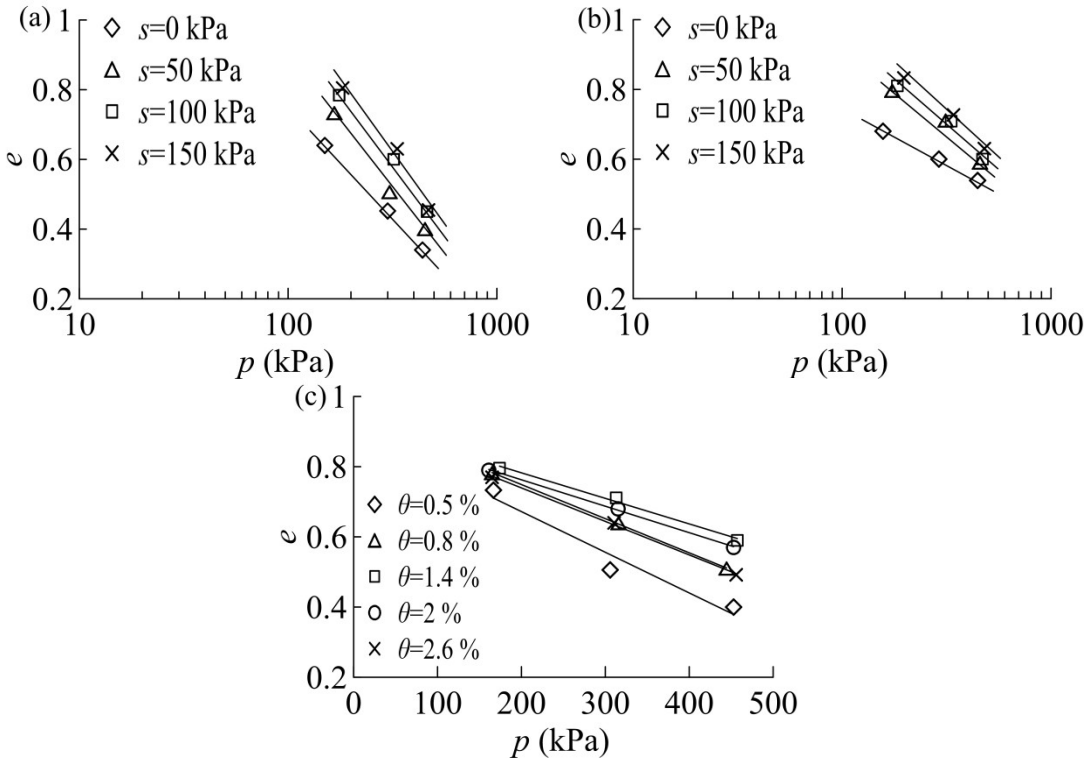

Fig. 8 CSLs in the plane of void ratio and net mean stress under different conditions: (a) θ=0.5 %; (b) θ=1.4 %; (c) s=50 kPa

Fig. 9 shows the CSLs in the plane of void ratio (e) and effective net mean stress (p') under different suctions, correspondingly the soluble salt content is 1.4 %. The CSLs of unsaturated undisturbed Ili loess in the e-p' plane were not showing normalization characteristic, which indicates that the unsaturated critical state characteristic can not be directly expressed only by the saturated critical state characteristic in e-p' plane.

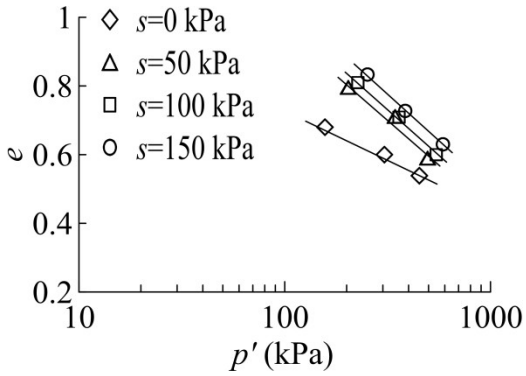

Fig. 9 CSLs in the plane of void ratio (e) and effective net mean stress (p') under different suctions (θ=1.4 %)

For a certain soluble salt content, the CSLs of unsaturated soil under different suctions are approximately parallel in the e-$lg(p)$ plane, and its mean value is taken as the slope of unsaturated CSL (λ_1). The corresponding slope of saturated CSL is recorded as λ_0. Fig. 10 shows the relationships of λ_0, λ_1 and soluble salt content (θ). It is found that both λ_0 and λ_1 first decrease and then increase with the increase of soluble salt content. When the soluble salt content is greater than 1.4 %, the compressibility increases on account of the thicker electric double layer for the saturated sample and the resultant lower normal and bending stiffnesses, due to the thicker cementation of crystallized salt for the unsaturated sample (Jiang et al., 2017). For a specific soluble salt content, the slope of unsaturated CSL (λ_1) is greater than that of saturated (λ_0). When the soluble salt content is greater than 1.4 %, the difference between λ_1 and λ_0 increases with the increase of soluble salt content. This is because the crystallized salt has a greater influence on the compressibility of the sample in comparison with solution concentration. As a result, when the soluble salt content is greater than the critical value of 1.4 %, the increase of compressibility of unsaturated soil is larger than that of saturated soil.

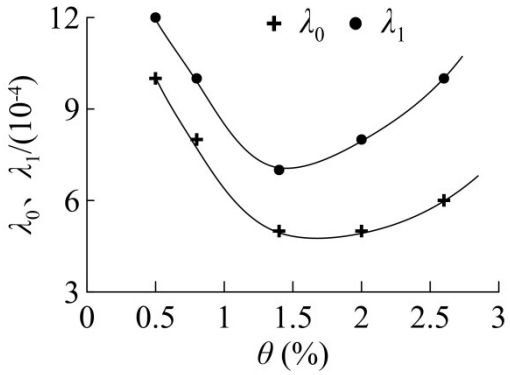

Fig. 10 Relationships of slopes of saturated (λ_0) and unsaturated (λ_1) CSL with the soluble salt content (θ)

Fig. 11 shows the relationship between the ratio of unsaturated void ratio to saturated void ratio (e/e_s) and degree of gas saturation (1-S_r) under different suctions, the corresponding soluble salt content is 0.8 %. For a specific soluble salt content, the test points gradually move to upper right with the increase of suction, indicating both the (1-S_r) and e/e_s increase as the increase of suction. This is because the greater suction causes the larger value of (1-S_r) due to the less content of water, and greater suction causes larger value of e/e_s because of stronger structure. In addition, the test points under different suctions uniformly distributed in a narrow band and can be approximately normalized as a single-valued nonlinear function, which is the relationship between the ratio of unsaturated void ratio to saturated void ratio (e/e_s) and the degree of gas saturation (1-S_r).

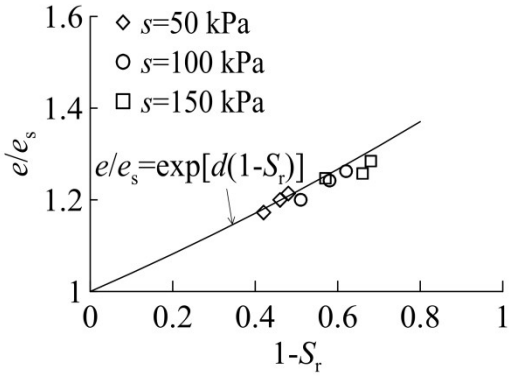

Fig. 11 Relationship of e/e_s and (1-S_r) under different suctions (θ=0.8 %)

Gallipoli et al. (2003) claimed that the ratio of unsaturated void ratio to saturated void ratio (e/e_s) under the same effective net mean stress (p') is the function of cementation coefficient (ζ),

which can be expressed as follows:

$$\begin{cases} e/e_s = 1 - g[1 - \exp(h\xi)] \\ \xi = f(s)(1 - S_r) \end{cases} \tag{11}$$

Where: g and h are soil parameters; for the saturated soil, 1-S_r=0, e/e_s=1. ξ is a dimensionless quantity reflecting the cementation of shrinkage membrane at the contact point of soil particles, which is mainly determined by the number of volume shrinkage membranes and the cohesive force within a single shrinkage membrane caused by suction. The above two aspects are expressed by the degree of gas saturation (1-S_r) and the ratio of normal binding force between unsaturated soil and saturated soil ($f(s)$). As the suction varies from 0 to infinity, the corresponding $f(s)$ changes monotonically from 1 to 1.5. The cementation coefficient ξ=1-S_r when $f(s)$=1, thus Eq. (11) is simplified as follows:

$$e/e_s = 1 - g\{1 - \exp[h(1 - S_r)]\} \tag{12}$$

Zhang et al. (2020) adopted Eq. (12) to fit the results of triaxial test controlling constant net mean stress and consolidation shear test, but he pointed out that the prediction was unsatisfactory when the cementation coefficient (ξ) is greater than 0.45, and the power equation was suggested as follows:

$$e/e_s = 1 + u(1 - S_r)^v \tag{13}$$

In this paper, the following equation is proposed to characterize the ratio of unsaturated void ratio to saturated void ratio (e/e_s) and the degree of gas saturation (1-S_r) :

$$e/e_s = \exp[d(1 - S_r)] \tag{14}$$

In Eq. (13) and (14): u, v and d are soil parameters, and the boundary conditions are satisfied: 1-

S_r=0 and e/e_s=1.

Eq. (12)~(14) were used to predict the test results of literature (Fang, & Feng, 2020), as shown in Fig. 12. It can be seen that, in comparison with Eq. (12) and (13) with two parameters, Eq. (14) has only one parameter d to describe the relationship between the ratio of unsaturated void ratio to saturated void ratio (e/e_s) and the degree of gas saturation ($1\text{-}S_r$) in the critical state. The test points with soluble salt content of 0.8 % in Fig. 11 are fitted by Eq. (14), as shown in Fig. 11. For a specific soluble salt content, Eq. (14) can characterize the relationship of e/e_s with ($1\text{-}S_r$) well under different suctions.

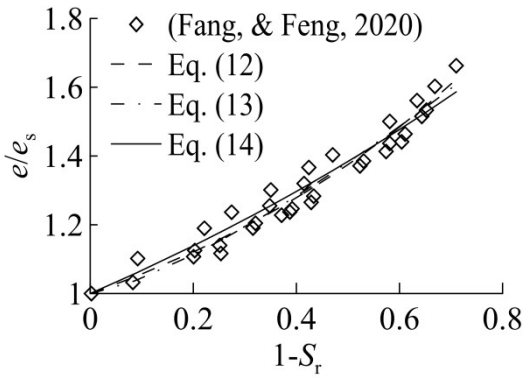

Fig. 12 The predictions of the test results of literature (Fang, & Feng, 2020)

Fig. 13 shows the relationship of e/e_s and ($1\text{-}S_r$) with different soluble salt contents in the critical state. The unsaturated undisturbed Ili loess under different conditions has quite different void ratio and degree of saturation in the critical state, but the test points with different soluble salt contents are all within a small region where e/e_s is equal to 1~1.4 in the e/e_s~($1\text{-}S_r$) plane.

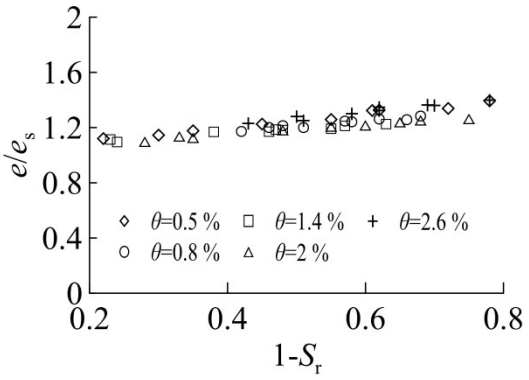

Fig. 13 The relationship of e/e_s and ($1\text{-}S_r$) with different soluble salt contents in the critical state

The soil parameter d is obtained by fitting the test points for different soluble salt contents. Fig. 14 shows the relationship between the soil parameter d and the soluble salt content. It can be seen that the soil parameter d first decreases and then increases as the increase of soluble salt content.

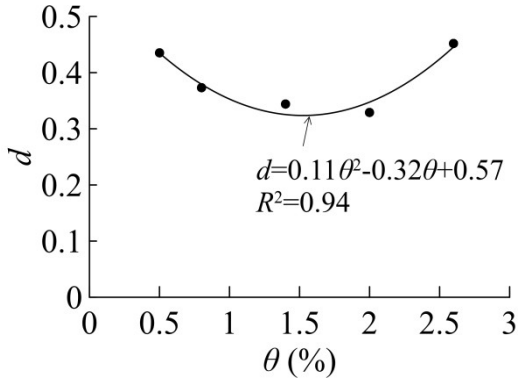

Fig. 14 The relationship of the parameter d and the soluble salt content

By substituting the equation of d expressed by soluble salt content into Eq. (14), the equation between the ratio of unsaturated void ratio to saturated void ratio (e/e_s) and the degree of gas saturation (1-S_r) for unsaturated undisturbed Ili loess considering the soluble salt content were obtained:

$$e/e_s=\exp\left[\left(0.11\theta^2-0.32\theta+0.57\right)\left(1-S_r\right)\right] \tag{15}$$

Where: θ is the soluble salt content (%).

The critical state void ratio of saturated soil (e_s) with a certain soluble salt content is calculated as follows:

$$e_s=N-\lambda_0 \ln p' \tag{16}$$

Where: N and λ_0 are the intercept and slope of the saturated CSL under the drainage shear test with a certain soluble salt content in the e-$ln(p')$ plane, respectively.

Therefore, for a certain effective net mean stress (p') and degree of saturation (S_r), the critical state void ratio e of unsaturated undisturbed Ili loess can be expressed as follows:

$$e=(N-\lambda_0 \ln p')\{\exp[(0.11\theta^2-0.32\theta+0.57)(1-S_r)]\} \quad (17)$$

4 Discussion

Fig. 15 shows the relationship of void ratio (e) and net mean stress (p) during shearing under different net confining pressures with the soluble salt content of 1.4 %. The corresponding NCLs are plotted in the e-p plane. It can be seen that, for the same soluble salt content and suction, the initial point of shear under different net confining pressures are all on the NCL and the CSL can be obtained by connecting the final points of shear in the e-p plane.

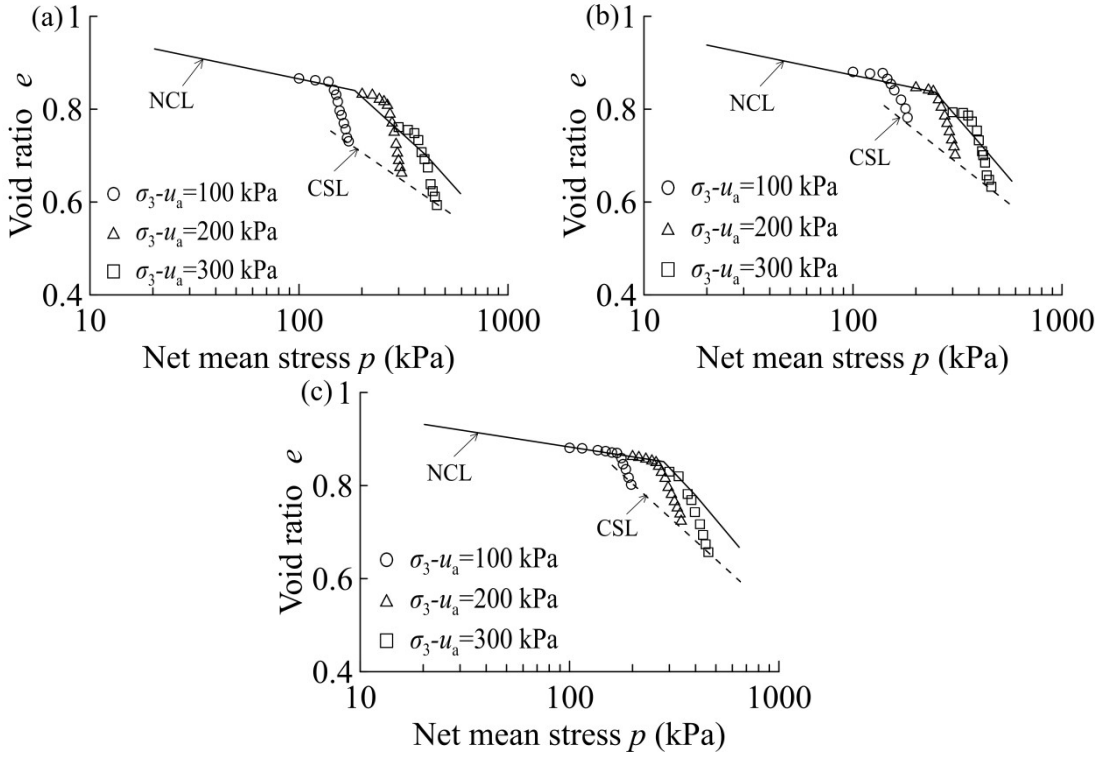

Fig. 15 Relationship of void ratio (e) and net mean stress (p) during shearing under different net confining pressures with the soluble salt content of 1.4 %: (a) s=50 kPa; (b) s=100 kPa; (c) s=150 kPa

As can be seen from Fig. 15, for a specific soluble salt content, the void ratio decreases first slowly and then rapidly with the increase of the net mean stress, which can be approximately expressed by two lines, and its intersection corresponds to the yield net mean stress of the isotropic compression (p_c). By comparing Fig. 15(a)~(c), the yield net mean stress of the isotropic compression (p_c) increases with the increase of suction, indicating that the larger suction delays

365 the void ratio to enter the rapidly decreasing stage due to the stronger soil structure.

366 When the net confining pressure is less than p_c, the change of void ratio after consolidation is
367 small because no yield occurs in the consolidation stage. On the contrary, when the net confining
368 pressure is greater than p_c, the void ratio after consolidation changes greatly. Before and after
369 shear yield, the void ratio decreases slowly along the NCL and rapidly away from the NCL,
370 respectively. This indicate that the volume under the triaxial shear stress condition is larger than
371 that under the isotropic compression stress condition for the same net mean stress.

372 **5 Conclusion**

373 In this paper, the compression curve (*e*-*p*), soil water characteristic curve (SWCC), critical
374 state lines (ie. CSLs in the plane of *p*-*q* and *e*-*p*) are normalized, and the normalization equations
375 considering the influence of soluble salt content are obtained. The main conclusions are
376 summarized as:

377 (1) The compression curves (*e*-*p*) under different suctions in the isotropic compression test
378 can be normalized by the ratio of the void ratio to initial void ratio (e/e_0) and the ratio of net mean
379 stress to yield net mean stress (p/p_c). Similarly, the SWCCs under different net mean stresses in the
380 triaxial shrinkage test can be normalized by the ratio of water content to saturated water content
381 (w/w_s) and the ratio of suction to air entry value (s/s_c). The normalized e/e_0-$lg(p/p_c)$ and w/w_s-$lg(s/s_c)$ curves both can be approximately expressed by exponential equation.

383 (2) In the consolidation shear test, for a specific soluble salt content, the unsaturated CSLs
384 under different suctions in the *p*-*q* plane can be normalized by the saturated CSL in the *p*-*q'* plane,
385 and the unsaturated CSLs under different suctions in the *e*-*p* plane can be normalized by the ratio
386 of unsaturated void ratio to saturated void ratio (e/e_s) and degree of gas saturation (1-S_r) under the
387 same effective net mean stress. For a specific soluble salt content, the slope of unsaturated CSL

(λ_1) is greater than that of saturated soil (λ_0) in the *e*-*p* plane and the difference between them gradually increases when the soluble salt content is greater than 1.4 %.

Acknowledgement

This work was supported by the State Key Research and Development Plan of China (Grant No. 2017YFC0405103), the National Natural Science Foundation of China (Grant No. 51978572) and the Key Research and Development Projects in Shaanxi Province of China (Grant No. 2017ZDXM-SF-074).

In addition, the authors are grateful to Associate Professor Minxia Guo for sample preparation, Associate Professor Haijun Hu for guiding the experimental operation, and teachers WuqingYan and Shunxiang Kang for management and help to the laboratory of Northwest A&F University.

Conflict of Interest Statement

We declare that we do not have any commercial or associative interest that represents a conflict of interest in connection with this work.

The following symbols are used in this paper:

A	Coefficient related to the compression stage
a, b, d, g, h, j, k, m, n, u, v, x, y, α and β	Soil parameters
c'	Effective cohesive (unit: kPa)
CSL	Critical state line
e, e_0 and e_s	Void ratio, initial void ratio and saturated void ratio, respectively
$f(s)$	Ratio of normal binding force between unsaturated soil and saturated soil
G_s	Specific gravity
I_p	Plasticity index (unit: %)
M	The slope of the critical state line of saturated soil
N	Intercept of the saturated critical state line under the drainage shear test (unit: kPa)

NCL	Normal compression line
p, p_c, p_h, p_f and p'	Net mean stress, yield net mean stress of the isotropic compression, vertical loading, shear failure net mean stress and effective net mean stress, respectively (unit: kPa)
q and q_f	Deviator stress and shear failure deviator stress, respectively (unit: kPa)
R^2	Correlation coefficient
S_r and 1-S_r	Degree of saturation and gas saturation, respectively (unit: %)
s and s_c	Suction and air entry value, respectively (unit: kPa)
u_a	Pore air pressure (unit: kPa)
w, w_0, w_l, w_p and w_s	Water content, initial water content, liquid limit, plastic limit and saturated water content, respectively (unit: %)
θ	Soluble salt content (unit: %)
ρ_d	Dry density (unit: g/cm^3)
σ_3 and σ_3-u_a	Small principal stress and net confining pressures, respectively (unit: kPa)
λ_1 and λ_0	Slopes of unsaturated and saturated critical state line in the e-$lg(p)$ plane, respectively
ξ	Cementation coefficient

Reference

Chen, C. L. , Zhang, D. F. , & Zhang, J. (2017). Influence of stress and water content on air permeability of intact loess. Canadian Geotechnical Journal, 54(9), 1221-1230. doi: 10.1139/cgj-2016-0186

Chen, Z. H. , Sun, S. G. , Fang, X. W. , Zhu, Y. Q. , & Xie, Y. (2007). Development and application of multi-function triaxial apparatus for soil. Journal of Logistical Engineering University, 23(4), 1–5. doi: 1672-7843(2007) 04-0001-05

Cheng, H. , Zhang, P. Z. , Spotl, C. , Edwards, R. L. , Cai, Y. J. , Zhang, D. Z. , Sang, W. C. , Tan, M. , & An, Z. S. (2012). The climatic cyclicity in semiarid-arid central Asia over the past 500, 000 years. Geophysical Research Letters, 39, 1705. doi: 10.1029/2011GL050202

Dettman, D. L. , Kohn, M. J. , Quade, J. , Ryerson, F. J. , Ojha, T. P. , & Hamidullah, S. (2001). Seasonal stable isotope evidence for a strong Asian monsoon throughout the past 10.7 m.y. Geology, 29(1), 31–34. doi: 10.1130/0091-7613(2001)029<0031:SSIEFA>2.0.CO;2

Dodonov, A. E. , & Baiguzina, L. L. (1995). Loess stratigraphy of Central Asia: Palaeoclimatic and palaeoenvironmental aspects. Quaternary Science Reviews, 14, 707–720. doi: 10.1016/0277-3791(95)00054-2

Fang, J. J. , & Feng, Y. X. (2020). Elastoplastic Model and Three-Dimensional Method for Unsaturated Soils. Shock And Vibration, 8592628. doi: 10.1155/2020/8592628

Gallipoli, D. , Gens, A. , Sharma, R. , & Vaunat, J. (2003). An elasto-plastic model for unsaturated soil incorporating the effects of suction and degree of saturation on mechanical behaviour. Geotechnique, 53(1), 123–135. doi: 10.1680/geot.53.1.123.37251

Gao, D. H. , Chen, Z. H. , Xing, Y. C. , Guo, N. , & Hu, S. X. (2018). Influence of net mean stress on permeability coefficient of unsaturated remolded loess. Chinese Journal of Geotechnical Engineering, 40(s1), 51–56. doi: 10.11779/CJGE2018S1009

Jiang, M. J. , He, J. , Wang, J. F. , Zhou, Y. P. , & Zhu, F. Y. (2017).Discrete element analysis of the mechanical properties of deep-sea methane hydrate-bearing soils considering interparticle bond thickness. Comptes Rendus Mecanique, 345(12), 868-889. doi: 10.1016/j.crme.2017.09.003

Li, C. X. , Song, Y. G. , & Wang, L. M. (2012). Distribution, age and dust sources of loess in the Ili Basin. Earth and Environment. 40(3), 314–320. doi: 10.1007/s11783-011-0280-z

Liu, D. D. , She, D. , & Mu, X. M. (2019). Water flow and salt transport in bare saline-sodic soils subjected to evaporation and intermittent irrigation with saline/distilled water. Land Degradation & Development, 30(10), 1204-1218. doi: 10.1002/ldr.3306

Machalett, B. , Oches, E. A. , Frechen, M. , Zoller, L. , Hambach, U. , Mavlyanova, N. G. , Markovic, S. B. , & Endlicher, W. (2008). Aeolian dust dynamics in central Asia during the Pleistocene: Driven by the long- term migration, seasonality, and permanency of the Asiatic polar front. Geochemistry Geophysics Geosystems, 9(8), 1–22. doi: 10.1029/2007GC001938

Niu, L. S. , Zhang, A. J. , Zhao, J. M. , Wang, Y. G. , & Zhao, Q. Y. (2020). Influences of soluble salt content on mechanical properties of Ili undisturbed loess. Chinese Journal of Geotechnical Engineering, 42(9), 1705-1714. doi: 10.11779/CJGE202009015

Nuth, M. , & Laloui, L. (2008). Effective stress concept in unsaturated soils: Clarification and validation of a unified framework. International Journal for Numerical and Analytical Methods in Geomechanics, 32(7), 771–801. doi: 10.1002/nag.645

Shao, S. J. , Wang, L. Q. , Shao, S. , & Wang, Q. (2017). Structural yield and collapse deformation of loess. Chinese Journal of Geotechnical Engineering, 39(8), 1357–1365. doi: 10.11779/CJGE201708001

Song, Y. G. , Chen, X. L. , Qian, L. B. , Li, C. X. , Li, Y. , Li, X. X. , Chang, H. , & An, Z. S. (2014). Distribution and composition of loess sediments in the Ili Basin, Central Asia. Quaternary International, 334, 61–73. doi: 10.1016/j.quaint.2013.12.053

Song, Y. G. , Zeng, M. X. , Chen, X. L. , Li, Y. , Chang, H. , An, Z. S. , & Guo, X. H. (2018). Abrupt climatic events recorded by the Ili loess during the last glaciation in Central Asia: Evidence from grain-size and minerals, Journal Of Asian Earth Sciences, 155, 58-67. doi: 10.1016/j.jseaes.2017.10.040

Sumner, M. E. , & Ravendra N. (1998). Sodic soils: distribution, properties, management and environmental consequences. New York: Oxford University Press.

Tian, K. L. , Wu, Y. Y. , Zhang, H. L. , Li, D. , Nie, K. Y. , & Zhang, S. C. (2018). Increasing wind erosion resistance of aeolian sandy soil by microbially induced calcium carbonate precipitation. Land Degradation & Development, 29, 4271–4281. doi: 10.1002/ldr.3176

Tsoar, H. , & Pye, K. (1987). Dust transport and the question of desert loess formation. Sedimentology, 34, 139–153. doi: 10.1111/j.1365-3091.1987.tb00566.x

Turner, R. E. , & Swenson, E. M. (2020). The Life and Death and Consequences of Canals and Spoil Banks in Salt Marshes. Wetlands, 1-9. doi: 10.1007/s13157-020-01354-w

Vandenberghe, J. , Renssen, H. , Van Huissteden, K. , Nugteren, G. , Konert, M. , Lu, H. Y. , Dodonov, A. , & Buylaert, J. P. (2006). Penetration of Atlantic westerly winds into Central and East Asia. Quaternary Science Reviews, 25, 2380–2389. doi: 10.1016/j.quascirev.2006.02.017

Viles, H. A. , & Goudie, A. S. (2007). Rapid salt weathering in the coastal Namib desert: Implications for landscape development. geomorphology, 85(1-2), 49–62. doi: 10.1016/j.geomorph.2006.03.025

Vinocur, B. , & Altman, A. (2005). Recent advances in engineering plant tolerance to abiotic stress: achievements and limitations. Current Opinion in Biotechnology, 16(2), 123–132. doi: 10.1016/j.copbio.2005.02.001

Wang, L. Q. , Shao, S. J. , & She, F. T. (2019). A New Method for Evaluating Loess Collapsibility and Its Application. Engineering Geology, 264, 105376. doi: 10.1016/j.enggeo.2019.105376

Wang, Y. G. , Zhang, A. J. , Ren, W. Y. , & Niu, L. S. (2019). Study on the Soil Water characteristic curve and its fitting model of Ili loess with high level of soluble salts. Journal of Hydrology, 578, 1–10. doi: 10.1016/j.jhydrol.2019.124067

Wang, Z. Y. , Tan, W. Y. , Yang, D. Q. , Zhang, K. Q. , Zhao, L. W. , Xie, Z. G. , Xu, T. , Zhao, Y. W. , Wang, X. N. , Pan, X. L. , & Zhang, D. Y. (2020). Mitigation of soil salinization and alkalization by bacterium-induced inhibition of evaporation and salt crystallization. The Science of the total environment, 755, 142511. doi: 10.1016/j.scitotenv.2020.142511

Welegedara, N. P. Y. , Grant, R. F. , Quideau, S. A. , & Mezbahuddin, S. (2020). Modeling salt redistribution and plant growth in reclaimed saline-sodic overburden upland forests: A case study from the Athabasca Oil Sands Region, Canada. Forest Ecology and Management, 472, 118154. doi: 10.1016/j.foreco.2020.118154

Yang, J. S. (2006). Recent evolution of soil salinization in China and its driving processes. In the 18th World Congress of Soil Science, 156, 3-4

Yang, S. L. , Forman, S. L. , Song, Y. G. , Pierson, J. , Mazzocco, J. , Li, X. X. , Shi, Z. T. , & Fang, X. M. (2014). Evaluating OSL-SAR protocols for dating quartz grains from the loess in Ili Basin, Central Asia. Quaternary Geochronology, 20, 78–88. doi: 10.1016/j.quageo.2013.11.004

Ye, W. (2000). The Mineral Characteristics of Loess and Depositing Environment In Yili Area, Xinjiang. Arid Land Geography, 17(4), 1–10. doi: 10.1007/s11769-000-0027-4

Ye, W. , Sadayo, Y. , & Zhao, X. Y. (2005). Comparison of the Sedimentary Features of Loess between the Westerly and Monsoon Regions in China. Arid Land Geography, 28(6), 789–794. doi: 10.3321/j.issn:1000-6060.2005.06.013

Zhang, A. J. , Xing, Y. C. , Hu, X. L. , Wang, H. T. , Guo, M. X. , Zhang, B. , & Gao, Y. P. (2016). Influence factors of strong self-weight collapsibility of Ili loess. Chinese Journal of Geotechnical Engineering, 38(s2), 117–122. doi: 10.11779/CJGE2016S2019

Zhang, D. F. , Wang, J. D. , Chen, C. L. , & Wang, S. H. (2020). The compression and collapse behaviour of intact loess in suction-monitored triaxial apparatus. Acta Geotechnica, 15(2), 529-548. doi: 10.1007/s11440-019-00829-3

Zhang, W. X. , Shi, Z. T. , Chen, G. J. , Liu, Y. , Niu, J. , Ming, Q. Z. , & Su, H. (2013). Geochemical characteristics and environmental significance of Talede loess-paleosol sequences of Ili Basin in Central Asia. Environmental Earth Sciences, 70(5),

491 2191–2202. doi: 10.1007/s12665-013-2323-1